This article has been accepted for publication in IEEE Transactions on Power Electronics. This is the author's version which has not been fully edited and content may change prior to final publication. Citation information: DOI 10.1109/TPEL.2024.3486048

Maximum Efficiency Tracking Control for Omnidirectional Wireless Power Transfer System Based on AdamW Algorithm

Zechi Chen, Xiangdong Sun, *Member, IEEE*, Weizhang Song, Patrick Wheeler, *Fellow*, *IEEE*, Jiang Liu, *Member, IEEE* and Biying Ren

***Abstract*—In order to increase the transmission efficiency of the receiving and transmitting coils of the omnidirectional wireless power transfer (OWPT) system in all-direction wireless transmission, and to reach the system's maximum efficiency output under constant output power, avoiding the power losses caused by additional DC/DC converters. This article proposes a maximum efficiency point tracking control algorithm based on AdamW algorithm. The system equivalent circuit model of three transmitting coils OWPT double-side LCC compensation network is established in this paper, and a maximum efficiency tracking control method based on AdamW is proposed. By changing the input voltage of the three transmitting coils and adjusting the current of the transmitting coils, the overall efficiency of the system can be optimized under constant power output. The effectiveness of the OWPT maximum transmission efficiency control method based on AdamW algorithm is verified by experiments, which can achieve the maximum efficiency output of the receiving coil at any position.**

***Index Terms*— Omnidirectional WPT system, Double side LCC compensation network, Maximum efficiency point tracking control, AdamW algorithm.**

I. Introduction

THE wireless power transfer system is frequently employed in many situations due to its ease and wireless cables. At present, the application scenarios of wireless transmission include implantable medical devices, portable electronic devices, and high-power car charging [1-2]. Due to the relatively simple objects of wireless transmission and the relatively stable coil positions, the charging methods of these devices are all fixed direction or positioning wireless transmission. However, for some special occasions, the position change of the receiving coil is relatively flexible, and the general charging method of fixed direction and position cannot effectively charge the equipment. The issue of changeable load position may be effectively resolved by the proposed omnidirectional wireless transmission system.

For the current common omnidirectional wireless power transfer system structures, there are bowl type [3], three-phase tubular collar type [4], rectangular transmitting coil type [5], and three-coil orthogonal type [6-7]. The characteristics of different types of wireless transmission systems vary, while the three-coil orthogonal type omnidirectional wireless transmission has a simple structure and relatively easy coil design. It is composed of three independent circular coils in a three-phase orthogonal manner. The three coils synthesize a new magnetic field direction for receiving coils in different directions by regulating the current flowing through each coil or the frequency of the current, so that receiving coils in any direction may efficiently receive the maximum transmission power.

However, while the switching frequency and transmitting coil current are fixed, variable receiving coil placements will significantly lower the system's transmission power and efficiency throughout the process of distance variation in the actual coil. Scholars have suggested various optimization techniques to aim for the system's optimum transmission power or efficiency.

Reference [8] introduces a method of fixing the working frequency of the transmitting coil at the resonant frequency of the coil, and proposes an equivalent load resistance matching method. By closed-loop adjusting the voltage of the front and rear DC/DC modules, the maximum efficiency tracking of the system is achieved. Although adding additional DC/DC converters may generate some additional power losses, the closed-loop system of the maximum efficiency point tracking (MEPT) control scheme can still achieve high overall efficiency in a wide range of coupling coefficients and load resistors. A scholar has proposed a WPT system that adds a boost converter at the receiving end. Establishing a mathematical model of the system shows that the duty cycle of the DC/DC converter and the derivative of the inverter input variable are constant. By adjusting the input voltage and output DC/DC duty cycle, MEPT of the system is achieved [9]. However, this relationship cannot be established for

Manuscript received May 17, 2024; revised July 30, 2024; revised September 10, 2024; accepted October 16, 2024. This work was supported in part by the National Natural Science Foundation of China under Grant 52477196 and Natural Science Foundation of Shaanxi under Grant 2023-JC-YB-390. (*Corresponding author*: Xiangdong Sun; e-mail: sxd1030@xaut.edu.cn).

Zechi Chen, Xiangdong Sun, Biying Ren and Weizhang Song are with the Electrical Engineering Department, Xi'an University of Technology, Xi'an, Shaanxi, China.

Jiang Liu is with the College of Electrical and Control Engineering, Xi'an University of Science and Technology and Xi'an Key Laboratory of Electrical Equipment Condition Monitoring and Power Supply Security, Xi'an, 710054, China.

Patrick Wheeler is with the Department of Electrical Engineering, The University of Nottingham, NG7 2RD Nottingham, U.K.

Authorized licensed use limited to: UNIVERSITY OF NOTTINGHAM. Downloaded on November 19,2024 at 15:19:26 UTC from IEEE Xplore. Restrictions apply.
© 2024 IEEE. Personal use is permitted, but republication/redistribution requires IEEE permission. See https://www.ieee.org/publications/rights/index.html for more information.

This article has been accepted for publication in IEEE Transactions on Power Electronics. This is the author's version which has not been fully edited and content may change prior to final publication. Citation information: DOI 10.1109/TPEL.2024.3486048

different compensation networks, and redesign is needed for different topologies. Reference [10] proposes a pulse density modulation (PDM) based MEPT to eliminate the problems of hard switching, low average efficiency, large DC voltage fluctuations, and increased power loss caused by DC/DC controllers in phase-shifting control. But the problem is that the modulation level of PDM cannot be too small. When the modulation level is too small, it can lead to unstable resonance state of the system. Moreover, when the operating frequency of the system is low, this problem will be more obvious, and the modulation method of PDM is more complex. The implementation of MEPT based on on-off control uses the low-frequency on-off duty cycle of inverters and active rectifiers as the control degree of freedom, but there are problems with low average efficiency and large fluctuations [11]. The phase shift based MEPT implementation uses the phase shift angle of the inverter and active rectifier as the control degree of freedom, but is affected by hard switching [12-13].

The maximum efficiency tracking control of OWPT system is the target optimization problem of the system. Common optimization algorithms include genetic algorithm (GA), particle swarm optimization (PSO), simulated annealing algorithm (SA), gradient descent algorithm (GD), stochastic gradient descent algorithm (SGD), adaptive moment estimation algorithm (Adam), etc.

The Adam algorithm is a stochastic optimization method proposed by Diederik P. Kingma and Jimmy Lei Ba in 2015 [14], which is a stochastic objective function one step optimization algorithm based on adaptive estimation of low order models [15]. A parameter identification method for underwater wireless transmission systems using the Adam algorithm is proposed in reference [16]. The Adam optimization algorithm is used to measure the single port impedance at different frequencies to identify the model parameters of the coupling coils in the wireless transmission system.

However, the L_2 regularization term in Adam is not as effective as SGD, resulting in a certain deviation in its convergence results compared to SGD. Therefore, some scholars have proposed a combination of Adam algorithm and weight decay regulation method, namely the AdamW algorithm, to ensure the accuracy of convergence [17]. The AdamW algorithm is an optimization algorithm of the Adam algorithm, which improves the weight decay processing method by separating weight decay from gradient updates. Weight decay is only applied to weight parameters and not to bias parameters.

The traditional MEPT implementation adds DC/DC converters on both the transmitting and receiving sides, but adding converters on both the transmitting and receiving sides can significantly affect the overall power of the system [18]. By controlling the three phase-shifting full bridges in the front stage, the voltage on the load can be controlled without adding a converter on both the transmitting and receiving sides. This can reduce the number of switching devices, the additional power loss of switching devices, and the complexity of control. Compared to adding a converter, using a phase-shifting full bridge controller has lower cost and higher efficiency.

In this paper, the current transmission power and efficiency are obtained by detecting the power of the receiving coil and the transmitting coils of the OWPT system. In order to achieve the maximum efficiency output of the load under a specific output power, a random gradient descent method based on AdamW is proposed to track and control the maximum efficiency. By changing the input voltage of the three transmitting coils, the current of the transmitting coils is adjusted. Thus, the synthetic magnetic field vector of the transmitting coil is changed to achieve the optimal control of the overall efficiency of the load coil under constant power output. Meanwhile, by avoiding the addition of DC/DC converters, the maximum transmission efficiency of the system is greatly increased.

The specific chapters of this paper are arranged as follows: The first part is the introduction of this paper, including the brief introduction of the research content of this paper. The second part is the mathematical model analysis of OWPT system and introduces the LCC compensation network. The third part is the principle of maximum efficiency tracking of OWPT system and the method of maximum efficiency tracking control. The fourth part is the experimental verification, through the experiment to verify the maximum efficiency tracking control method of OWPT effectiveness, the last part is the summary of the paper.

II. Modeling And Analysis Of OWPT System

The OWPT system consists of three inverters connected to three transmitting coils by the compensation networks, and the receiving coil is connected to the load through a rectifier. The system can adjust the current flowing through the transmitting coils by changing the input voltage of the three transmitting coils to control the current of the receiving coil. The information at the transmitting and receiving sides are transmitted wirelessly. By detecting the voltage or power on the load side, constant power and maximum efficiency point tracking control of the entire system can be achieved.

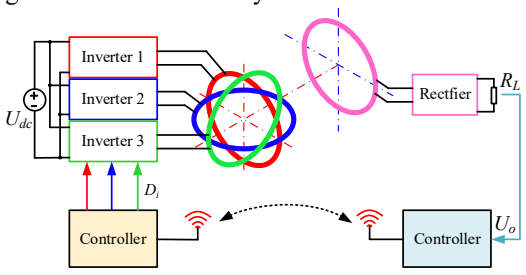

Fig. 1. OWPT system structure diagram.

When all coils of the omnidirectional wireless transmission system adopt SS compensation network, due to the mutual inductance between the transmitting coil and the receiving coil, the current of the transmitting coil 1 is reflected back to the transmitting coil 2 through the receiving coil. However, when the coupling coefficient between the transmitting coil 2

Authorized licensed use limited to: UNIVERSITY OF NOTTINGHAM. Downloaded on November 19,2024 at 15:19:26 UTC from IEEE Xplore. Restrictions apply.
© 2024 IEEE. Personal use is permitted, but republication/redistribution requires IEEE permission. See https://www.ieee.org/publications/rights/index.html for more information.

This article has been accepted for publication in IEEE Transactions on Power Electronics. This is the author's version which has not been fully edited and content may change prior to final publication. Citation information: DOI 10.1109/TPEL.2024.3486048

and the receiving coil is small, the current on the transmitting coil is large, and the system cannot function normally.

In order to solve the problem of system malfunction, scholars have proposed using high-order compensation networks such as LCC, LCL, etc. as compensation networks for the receiving and transmitting coils. The LCC-LCC compensation network and its tuning method are independent of the coupling coefficient between the two coils and the load conditions, which means that the system can operate at a constant switching frequency. The equivalent model of the system when using double side LCC (DS-LCC) compensation network is shown in Fig. 2.

In Fig. 2, the U_{dc} is the DC side input voltage, I_{dc} is the DC side input current. U_{p1}, U_{p2}, and U_{p3} are the input voltages of the transmitting coils. I_{p1}, I_{p2}, and I_{p3} are the current of the transmitting coils. I_{f1}, I_{f2}, and I_{f3} are the current of the LCC compensation network of transmitting coils. I_{p4} is the current of the receiving coil. I_{f4} is the current of the LCC compensation network of receiving coil. L_{p1}, L_{p2}, L_{p3}, and L_{p4} are the self-inductance of each coil. C_{p1}, C_{p2}, C_{p3}, and C_{p4} are the resonant capacitance of each coil. R_{p1}, R_{p2}, R_{p3}, and R_{p4} are the internal resistance of the transmitting coils. L_{f1}, L_{f2}, L_{f3}, and L_{f4} are the LCC inductance. C_{f1}, C_{f2}, C_{f3}, and C_{f4} are the LCC capacitance. The receiving side is the rectifier circuit Q_{41}~Q_{44} and load R_L. For the convenience of analysis, the rectifier and load can be equivalent to R_{eq}, which can be approximated as $R_{eq} = 8R_L/\pi^2$.

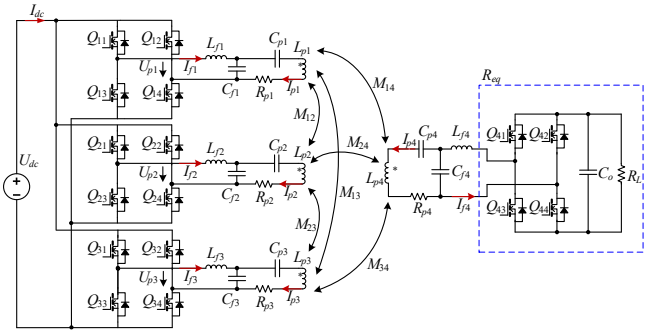

Fig. 2. DS-LCC compensation network of three-coil OWPT system.

Three phase-shifting full-bridge inverters are composed of Q_{i1}~ Q_{i4}, i = 1, 2, 3, sharing the same input DC power supply. The output voltage of inverter $U_{p1\sim3}$ can be controlled by the phase-shifting angle of its inverter, thereby controlling the current of the three transmitting coils.

M_{14}, M_{24}, and M_{34} are mutual inductance between the three transmitting and receiving coils. M_{12}, M_{23}, and M_{13} are mutual inductance between the three emission coils. To simplify the analysis, assume that the mutual inductance between transmitting coils 1, 2, and 3 is approximately 0 [19-20], and analyze the system using a single transmitting coil 1 and a receiving coil.

Due to the ability to achieve zero current switching (ZCS) of the primary side switch and constant coil current output in a LCC network [21], the design objectives of the LCC compensation network should be

$$\begin{cases} L_{fi}C_{fi} = 1/\omega_0^{\,2} \\ \left(L_{pi} - L_{fi}\right)C_{pi} = 1/\omega_0^{\,2} \end{cases}, i = 1,2,3,4 \tag{1}$$

Where, ω_0 is the resonant center angular frequency.

In the compensation network conditions of LCC, in order to simplify the analysis, a single transmitting coil 1 and a receiving coil are used to analyze the system. According to the KVL equation, there are

$$\begin{bmatrix} A & 0 & 0 & j/\omega C_{f1} \\ 0 & B & j/\omega C_{f4} & 0 \\ 0 & j/\omega C_{f4} & C & -j\omega M_{14} \\ j/\omega C_{f1} & 0 & j\omega M_{14} & D \end{bmatrix} \begin{bmatrix} I_{f1} \\ I_{f4} \\ I_{p4} \\ I_{p1} \end{bmatrix} = \begin{bmatrix} U_{p1} \\ 0 \\ 0 \\ 0 \end{bmatrix} \tag{2}$$

Where, ω is the angular frequency.

$$\begin{cases} A = j\omega L_{f1} + 1/j\omega C_{f1} \\ B = j\omega L_{f4} + 1/j\omega C_{f4} + R_{p4} + R_{eq} \\ C = j\omega L_{p4} + 1/j\omega C_{f4} + 1/j\omega C_{p4} \\ D = j\omega L_{p1} + 1/j\omega C_{f1} + 1/j\omega C_{p1} + R_{p1} \end{cases} \tag{3}$$

The transfer function between output voltage and input voltage is

$$G_{DS-LCC} = \frac{M_{14}R_{eq}/j\omega C_{f1}C_{f4}}{Z_1\left(Z_2 + 1/j\omega C_{f1}\right)\left(Z_3 + j\omega M_{14}\right)\left(Z_4 + 1/j\omega C_{f4}\right)} \tag{4}$$

$$Z_{in} = 1/Z_1 \tag{5}$$

The parameters in (4) are shown in (6).

$$\begin{cases} Z_4 = R_{eq} + j\omega L_{f4} \\ Z_3 = R_{p4} + 1/j\omega C_{p4} + j\omega\left(L_{p4} - M_{14}\right) + Z_4/\left(1 + Z_4 j\omega C_{f4}\right) \\ Z_2 = R_{p1} + 1/j\omega C_{p1} + j\omega\left(L_{p1} - M_{14}\right) + Z_3 j\omega M_{14}/\left(j\omega M_{14} + Z_3\right) \\ Z_1 = j\omega L_{f1} + Z_2/\left(1 + Z_2 j\omega C_{f1}\right) \end{cases} \tag{6}$$

When the system adopts the DS-LCC compensation network, the transmission characteristic curve can be obtained when the coupling system between coils is different, as shown in Fig. 3 (a).

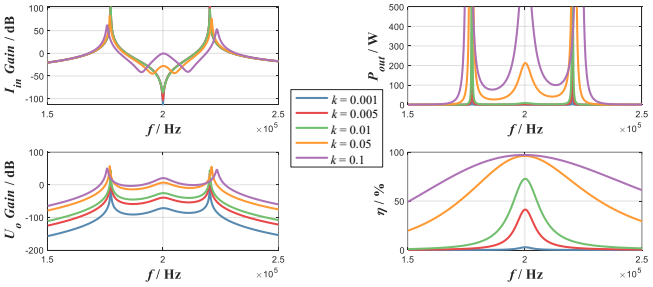

(a) (b)

Fig. 3. Transmission characteristic of DS-LCC compensation network. (a) Input current and output power. (b) Transmission power and efficiency curve.

From the output voltage and input current gain, it can be seen that when the transmitting and receiving coils are close to each other (larger coupling coefficient), the overall output gain of the system has a better level at the resonance frequency, and the output power of the system can reach a larger level with respect to that of the SS compensation network. The output power as well as the transmission efficiency of the system is shown in Fig. 3 (b), it can be seen that when the

Authorized licensed use limited to: UNIVERSITY OF NOTTINGHAM. Downloaded on November 19,2024 at 15:19:26 UTC from IEEE Xplore. Restrictions apply.
© 2024 IEEE. Personal use is permitted, but republication/redistribution requires IEEE permission. See https://www.ieee.org/publications/rights/index.html for more information.

This article has been accepted for publication in IEEE Transactions on Power Electronics. This is the author's version which has not been fully edited and content may change prior to final publication. Citation information: DOI 10.1109/TPEL.2024.3486048

distance between the transmitting and receiving coils is relatively close, there is no frequency splitting in the system, and high transmission power and efficiency can still be achieved at the central frequency. When the distance between coils is slightly far, the output power and transmission efficiency will decrease simultaneously due to the small coupling coefficient. However, by adjusting the input voltage of the transmitting coil, power control of the receiving coil can be achieved.

There is a certain coupling between orthogonal transmitting coils, but the coupling coefficient between the coils is very small. From the characteristics of the LCC-LCC compensation network, it can be seen that when the coupling coefficient is small, the gain of the induced output voltage is also small, so the influence between the orthogonal coils can be ignored [19].

III. Maximum Efficiency Point Tracking for OWPT System

The characteristics of wireless Electric power transmission based on DS-LCC compensation network are extended to omnidirectional wireless electric power transmission. Since the current I_{p4} flowing on the receiving coil is the sum of the induced currents of the three transmitting coils, according to this feature, the equation of state of the system is

$$\begin{bmatrix} A_1 & 0 & 0 & B_1 \\ 0 & A_2 & 0 & B_2 \\ 0 & 0 & A_3 & B_3 \\ j\omega M_{14} & j\omega M_{24} & j\omega M_{34} & C \end{bmatrix} \begin{bmatrix} I_{p1} \\ I_{p2} \\ I_{p3} \\ I_{p4} \end{bmatrix} = \begin{bmatrix} U_{p1} \\ U_{p2} \\ U_{p3} \\ 0 \end{bmatrix} \tag{7}$$

The parameters in (7) is shown in (8).

$$\begin{cases} A_i = \left(1/j\omega C_{pi} + j\omega L_{pi} + R_{pi}\right)\left(1 - L_{fi}C_{fi}\omega^2\right) + j\omega L_{fi} \\ B_i = \left(1 - L_{fi}C_{fi}\omega^2\right) j\omega M_{i4} \\ C = j\omega L_{p4} + 1/j\omega C_{p4} + R_{p4} + D \\ D = \left(j\omega L_{f4} + R_{eq}\right) \Big/ \left[1 + j\omega C_{f4}\left(j\omega L_{f4} + R_{eq}\right)\right] \end{cases} \tag{8}$$

Where, i = 1, 2, 3. The current flowing on the transmitting and receiving coils are

$$\begin{cases} I_{p4} = \sum_{i=1}^{3} \dfrac{U_{pi} j\omega M_{i4}}{A_i} \Big/ \left(\sum_{i=1}^{3} \dfrac{B_i j\omega M_{i4}}{A_i} - C \right) \\ I_{pi} = \left(U_{pi} - B_i I_{p4}\right) \Big/ A_i, i = 1,2,3 \end{cases} \tag{9}$$

At this point, the output voltage is

$$U_o = \left[I_{p4}\left(j\omega L_{p4} + R_{p4} + \frac{1}{j\omega C_{p4}} \right) + \sum_{i=1}^{3} I_{pi} j\omega M_{i4} \right] \left(\frac{R_{eq}}{R_{eq} + j\omega L_{f4}} \right) \tag{10}$$

The input and output power and transmission efficiency of the system are

$$\begin{cases} P_o = \mathrm{abs}\left(U_o\right)^2 \Big/ R_{eq} \\ P_{in\_tx} = \sum_{i=1}^{3} U_{pi} I_{fi} \\ P_{loss} = P_{inv} + P_{com} + P_{coil\_tx} + P_{coil\_rx} \\ \eta = P_o \Big/ \left(P_{in\_tx} + P_{inv}\right) \end{cases} \tag{11}$$

Where, $I_{fi} = I_{pi}\left(C_{fi}/C_{pi} + 1 - L_{pi}C_{fi}\omega^2\right) - I_{p4}C_{fi}M_{i4}\omega^2$, P_{in_tx} is the input power of the transmitting coil. P_{loss} is the overall loss of the system. This mainly includes inverter loss P_{inv}, transmitting coil loss $P_{coil\_tx} = \sum_{i=1}^{3} {I_{pi}}^2 R_{pi}$, receiving coil loss $P_{coil\_rx} = {I_{p4}}^2 R_{p4}$, and compensating network loss P_{com}. Due to the minimal impact of the internal resistance of the compensation network on the system, P_{com} was ignored in the subsequent analysis. The losses of the transmitting coil and the receiving coil only consider the internal resistance loss.

$$\begin{aligned} P_{inv} = {} & \frac{1}{2\pi}\int_0^{\pi} {I^2}_{ds(on)} R_d \tau(t)\, dt + \frac{1}{2} U_{dc} I_{ds(on)} \left(t_{on} + t_{off}\right) f_0 \\ & + \frac{1}{2} U_{dc} C_{oss} f_0 \end{aligned} \tag{12}$$

The main power loss of the inverter P_{inv} is (12), which includes the turn-on loss and the switching loss. The turn-on loss is determined by the conduction resistance of the switching transistor and the current flowing through it. When the current is basically constant, the turn-on loss at this time also remains basically unchanged. The switching loss is determined by the switching frequency f_0, the switching time (t_{on}+t_{off}), and the output capacitance C_{oss} of the switching transistor.

A. MEPT for Coil Position Changes

Fig. 4 is the schematic diagram of the load coil rotating around the Z-axis of the transmitting coils. The three transmitting coils of the OWPT system are 1, 2, and 3, respectively. The transmission coils 1, 2, and 3 are perpendicular to the X-axis, Y-axis, and Z-axis, respectively. The angle between the receiving coil and the Z-axis is θ, the angle between its projection and the X-axis is φ.

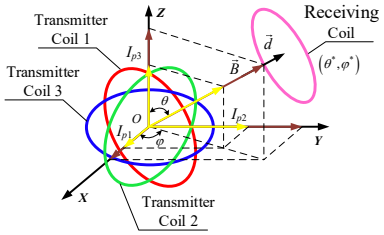

Fig. 4. Schematic diagram of coil position in OWPT system.

When the receiving coil rotates around the transmitting coil, the mutual inductance M_{14}, M_{24} and M_{34} between the receiving coil and the transmitting coils changes, i.e., the coupling coefficients k_{14}, k_{24} and k_{34} also change, where $k_{i4} = M_{i4} / \sqrt{L_{pi}L_{p4}}$. And when the coupling coefficients between the transmitting and receiving coils are changed, according to (11), it can be seen that the voltage on the load can be maintained to a constant power by changing the input voltages of the different transmitting coils.

Taking the change of the coupling coefficient of the system when the position of the receiving coil is changed as an example, as shown in Fig. 5, the curves of the input voltage and constant output power 20 W of the system with different coupling coefficients of the receiving coil and the transmitting

Authorized licensed use limited to: UNIVERSITY OF NOTTINGHAM. Downloaded on November 19,2024 at 15:19:26 UTC from IEEE Xplore. Restrictions apply.
© 2024 IEEE. Personal use is permitted, but republication/redistribution requires IEEE permission. See https://www.ieee.org/publications/rights/index.html for more information.

This article has been accepted for publication in IEEE Transactions on Power Electronics. This is the author's version which has not been fully edited and content may change prior to final publication. Citation information: DOI 10.1109/TPEL.2024.3486048

coil, as well as the curves of the transmission efficiency of the system with different input voltages under the constant output power are shown, respectively. In Fig. 5 (a, b) k_{14} = 0.0345, k_{24} = 0, k_{34} = 0. In Fig. 5 (c, d) k_{14} = 0.027, k_{24} = 0.025, k_{34} = 0. In Fig. 5 (e, f) k_{14} = 0.02, k_{24} = 0.021, k_{34} = 0.023.

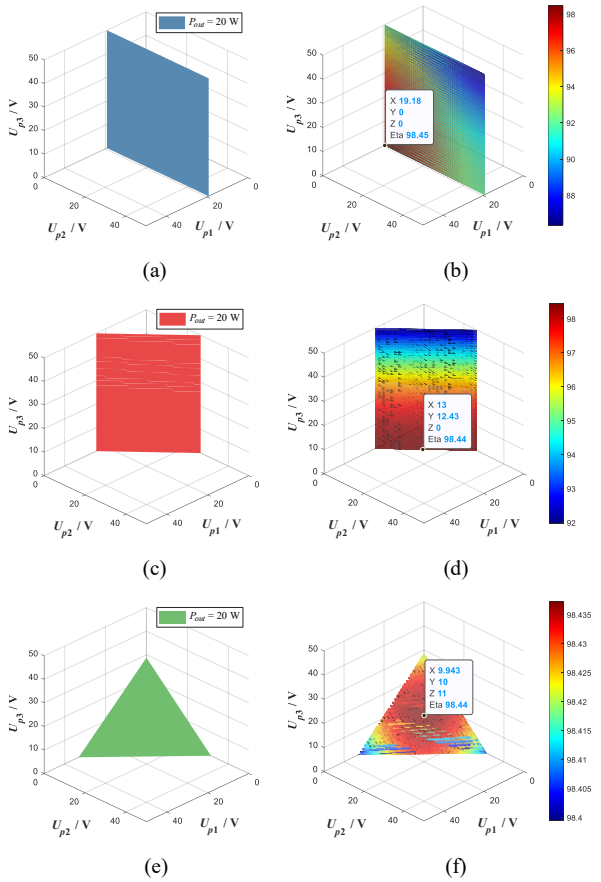

Fig. 5. The input voltage and constant output power curves of the system and the transmission efficiency curves. (a, c, e) constant output power curves. (b, d, f) transmission efficiency curves.

It can be noticed that constant power control of the output load can be achieved by combining the input voltages when the receiving coil is in a situation where the mutual inductance of the three transmitting coils is not equal to 0, and constant power of the system can be achieved at any voltage on the Fig. 5 (a, c, e). However, under constant output power, the transmission efficiency of the system varies with different input voltages. From Fig. 5 (b, d, f), it can be seen that the maximum transmission efficiency of the system is a unique point.

B. MEPT for Output Power and Load Changes

In order for the system to achieve constant power output and maximum efficiency under different conditions, the transmission characteristics of the system under different output power and loads were also considered. Fig. 6 (a, b), different output power, 20 W and 40 W respectively. Fig. 6 (c, d), different load, 5Ω and 20 Ω respectively.

As can be seen from Fig. 6 (a), when the output power of the system changes, the system can reach the maximum transmission efficiency under a certain input voltage. At this point, the coupling coefficient of the system are k_{14} = 0.0353, k_{24} = 0.012, and k_{34} = 0. However, the ratio of input voltage is different at this time. When the load changes, as shown in Fig. 6 (c, d), the output power remains unchanged, and the proportion of input voltage when the system reaches the maximum transmission efficiency is also different.

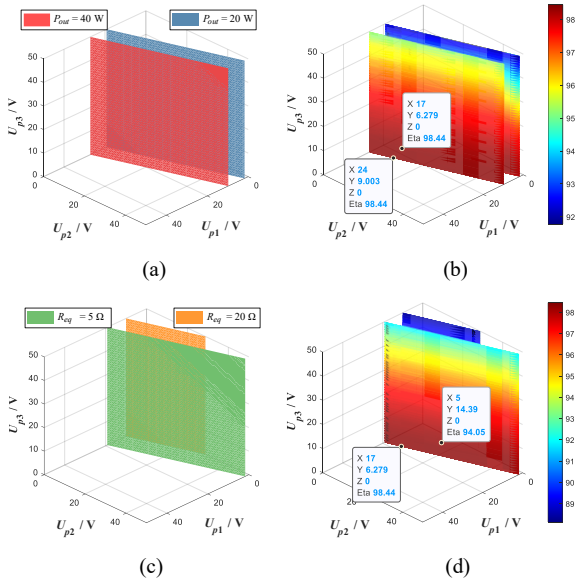

Fig. 6. The transmission characteristics of the OWPT system under different loads and output power. (a, b). Input voltage variation curve under different constant output. (c, d). Curve of input voltage and efficiency with constant output power under different loads.

The combination of the transmitting coil's input voltage to achieve maximum transmission efficiency is different, as shown in Fig. 6 (b), when the positions of the transmitting and receiving coils remain unchanged and the constant power output is maintained under different loads. This indicates that the maximum efficiency point is not proportional to the current flowing through the transmitting coil, but is related to multiple reasons.

C. Implementation of MEPT algorithm

According to the previous analysis, it can be seen that there are various combinations of input voltage that can achieve constant output power of the load. However, there must be a suitable voltage combination to ensure that the system maintains a constant power output and can achieve maximum transmission efficiency. The search for input voltage at this efficiency point has become an urgent issue to be addressed in this article.

According to (11), it can be obtained that the maximum transmission efficiency point of the system is the unique solution, hence the maximum efficiency point tracking problem is the problem of solving the maximum value of the system. Optimization algorithms such as GA, SA, PSO, etc. are widely used to solve complex optimization problems, especially in situations where the search space is large or traditional methods are difficult to solve. Although their goal is to find the optimal or approximate optimal solution to the problem, there are differences in convergence speed, algorithm implementation methods, and complexity. However,

Authorized licensed use limited to: UNIVERSITY OF NOTTINGHAM. Downloaded on November 19,2024 at 15:19:26 UTC from IEEE Xplore. Restrictions apply.
© 2024 IEEE. Personal use is permitted, but republication/redistribution requires IEEE permission. See https://www.ieee.org/publications/rights/index.html for more information.

This article has been accepted for publication in IEEE Transactions on Power Electronics. This is the author's version which has not been fully edited and content may change prior to final publication. Citation information: DOI 10.1109/TPEL.2024.3486048

these biomimetic algorithms often have high algorithm complexity and are difficult to implement in DSP.

The AdamW algorithm based on the improved gradient descent method is relatively easy and has good convergence effect, and is currently widely used in neural networks. The basic principles of the Adam algorithm are AdaGrad and RMSProp, which combine the main advantages of the two algorithms and also make some innovations. AdamW algorithm adds weight decay to the Adam algorithm, subtracting a gradient from each updated gradient to restrict parameter values from being too large.

The AdamW algorithm is easy to implement, has high computational efficiency, small memory requirement, intuitive interpretation of hyperparameters, and basically requires very little parameter adjustment. Although the current AdamW algorithm is often used for hyperparameter optimization of neural networks, it is essentially a kind of gradient descent method, which is also suitable for traditional convex optimization problems. Compared with other gradient descent methods, AdamW algorithm has faster convergence speed and is simple to realize, and can better handle sparse gradients and naturally have annealing effect.

Its convergence speed and final convergence effect are faster than those of conventional gradient descent techniques. AdamW not only calculates the adaptive parameter learning rate based on the first-order moment mean, as in the RMSProp algorithm, but also fully utilizes the second-order moment mean of the gradient (i.e. uncentered variance). Specifically, the algorithm calculates the exponential moving average of the gradient, and the hyperparameters β_1 and β_2 control the decay rate of these moving averages. The initial value of the moving mean and the β_1 and β_2 values are close to 1 (recommended value), so the deviation of the moment estimation is close to 0. The bias is improved by first calculating the biased estimate and then calculating the bias corrected estimate.

The optimization objectives of this article are

$$\begin{cases} f(\theta) = -\eta_{\min}(U_{dci}), i = 1,2,3 \\ \text{s.t. } P_o = \text{CONST} \end{cases} \tag{13}$$

Since the input voltages of the three inverters on the transmitting side are shared, it is impossible to adjust the input voltages of each inverter independently. However, the output voltage of the inverter can be controlled by phase-shifting modulation. Output voltage U_{pi} is controlled by phase shift angle D_{pi}. At this time, the optimization problem of the system becomes

$$\begin{cases} f(\theta) = -\eta_{\min}(D_{pi}), i = 1,2,3 \\ \text{s.t. } P_o = \text{CONST} \end{cases} \tag{14}$$

The specific implementation pseudocode of the AdamW algorithm is shown in Table I.

Among the pseudocode, $f(\theta)$ represents the transmission efficiency of the system -$\eta_{\min}$. $f(\theta)$ represents a differentiable random scalar function with respect to parameter θ, which is the phase shift duty D_{pi}. Firstly, initialize the optimization parameters of the system and set the default learning rate α = 0.001, β_1 is the exponential decay rate of first-order moment estimation, β_2 is the exponential decay rate of second-order moment estimation. θ_0 is the initial input parameter of the system, m_0 and v_0 are the first-order moment estimation (Momentum term) and second-order moment estimation (RMSProp term) of the system, respectively. $\hat{m}$ and $\hat{v}$ are the corrected first-order moment and second-order moment deviation values, respectively.

The specific implementation process of AdamW algorithm is as follows: the system is divided into 7 steps in the search and update process.

1. Update on the number of iterations t.
2. Calculate the gradient value of the system.
3. Calculate the estimation m_i of the first moment at the current moment.
4. Calculate the estimation v_i of the second-order moment at the current time.
5. The default initial value of the first-order moment estimation is 0. In order to reduce the bias to 0, the first-order moment estimation value is corrected.
6. Use the same method to correct the second-order moment estimation.
7. Calculate the gradient descent based on first-order and second-order moment estimation, and use the same to regularize all weights and decouple gradient descent from weight decay.

TABLE I
PSEUDOCODE FOR ADAMW ALGORITHM

AdamW. Where g_i indicates the current gradient. g_i^2 indicates the HAdamWard product $g_i^2 = g_i \odot g_i$. Good default settings for the problems are $\alpha = 0.001$, $\beta_1 = 0.9$, $\beta_2 = 0.999$ and $\varepsilon = 10^{-8}$. All operations on vectors are elementwise. With β_{t1} and β_{t2} denote β_1 and β_2 to the power i. λ defines the rate of the weight decay per step.

Initial α: Learning stepsize
$\beta_1, \beta_2 \in [0, 1)$: Exponential decay rates for the moment estimates
$f(\theta)$: Stochastic objective function with parameters θ, where $f(\theta)$ means -η
θ_0: Initial parameter vector
$m_0 \leftarrow 0$ (Initialize 1st moment vector)
$v_0 \leftarrow 0$ (Initialize 2nd moment vector)
$i \leftarrow 0$ (Initialize timestep)

while θ_i not converged **do**
$i \leftarrow i+1$
$g_i \leftarrow \nabla_\theta f_{i-1}(\theta)$ (Get gradients w.r.t. stochastic objective at timestep i)
$m_i \leftarrow \beta_1 m_{i-1} + (1-\beta_1) g_i$ (Update biased first-order moment estimate)
$v_i \leftarrow \beta_2 v_{i-1} + (1-\beta_2) g_i^2$ (Update biased second-order moment estimate)
$\hat{m}_i \leftarrow m_i / (1-\beta_1^i)$ (Compute bias-corrected first-order moment estimate)
$\hat{v}_i \leftarrow v_i / (1-\beta_2^i)$ (Compute bias-corrected second-order moment estimate)
$\theta_i \leftarrow \theta_{i-1} - \alpha \hat{m}_i / (\sqrt{\hat{v}_i} + \varepsilon) - \lambda \theta_{i-1}$ (Update parameters)

end while

return θ_i (Resulting parameters)

The AdamW algorithm carefully picks the step size when updating rules, which is an important characteristic. The

Authorized licensed use limited to: UNIVERSITY OF NOTTINGHAM. Downloaded on November 19,2024 at 15:19:26 UTC from IEEE Xplore. Restrictions apply.
© 2024 IEEE. Personal use is permitted, but republication/redistribution requires IEEE permission. See https://www.ieee.org/publications/rights/index.html for more information.

This article has been accepted for publication in IEEE Transactions on Power Electronics. This is the author's version which has not been fully edited and content may change prior to final publication. Citation information: DOI 10.1109/TPEL.2024.3486048

momentum term estimates the mean value of the gradient, gradually canceling out the positive and negative step sizes of the gradient in the vertical direction, and gradually accumulating the step sizes in the horizontal direction, minimizing oscillations and accelerating the learning rate. The RMSProp concept is that for gradients with high fluctuations, their variance is also large. Therefore, the gradient for gradient descent is calculated by dividing the gradient by the square root of the second-order distance, which likewise reduces the step size on the vertical axis while increasing the step size on the horizontal axis.

Fig. 7 shows the convergence curves of GD algorithm and AdamW algorithm at the same initial learning step size. Fig. 7 (a) is the convergence curve of power from 0 to a constant output power, and (b) is the efficiency convergence curve, ultimately converging to the maximum efficiency point. At this point, the coupling coefficient of the system are k_{14} = 0.0353, k_{24} = 0.012, and k_{34} = 0.

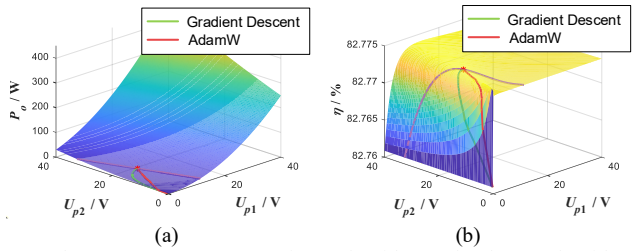

(a) (b)

Fig. 7. The Convergence curves of GD algorithm and AdamW algorithm at the same initial learning rate. (a) power convergence curve. (b) efficiency convergence curve.

Fig. 8 shows the curve of system convergence speed and error. By comparing the convergence speeds of gradient descent algorithm, RMSprop, Adam, and AdamW, it can be seen that AdamW algorithm has a faster convergence speed and better performance compared to other algorithms.

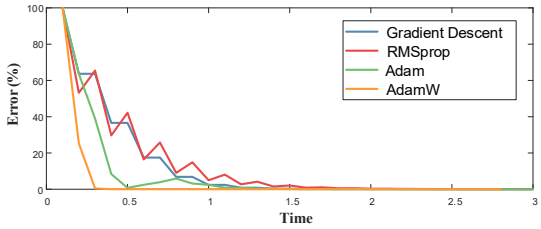

Fig. 8. The Convergence curves of GD, RMSprop, Adam and AdamW algorithm at the same initial learning rate.

Compared to traditional gradient descent methods, AdamW introduces first-order moment and second-order distance estimation by combining RMSProp and Momentum, which can be seen as an estimation of the gradient's signal-to-noise ratio (SNR). SNR usually gradually decreases until it approaches 0 with training, resulting in a smaller effective step size and achieving automatic annealing of the step size.

IV. Experimental Verification

The overall control block diagram of the system is shown in Fig. 9. The phase-shifting inverters of three transmitting coils share one input DC source. The receiving side sends data to the transmitting side through a wireless data transmission chip. The transmitting side tracks the maximum efficiency point using the AdamW algorithm, adjusts the duty cycle of the three phase-shifting inverters, and changes the current of the transmitting coils.

In order to ensure the correctness and feasibility of the proposed method, an experimental prototype of OWPT was constructed in this paper, as shown in Fig. 10. The inverter on the transmitting side of the experimental platform is a three-phase full-bridge composed of SiC devices, and the receiving side is a synchronous rectification circuit composed of SiC devices. SiC MOSFET is C2M0080120D from Wolfspeed. The driver of MOSFET is TI's UCC21520. The main controller is a DSP with a model of TMS320F28379D. The transmitting and receiving sides communicate wirelessly by Bluetooth, and the Bluetooth chips are ESP32C3 from Espressif. The specific parameters of the experimental platform are shown in Table II.

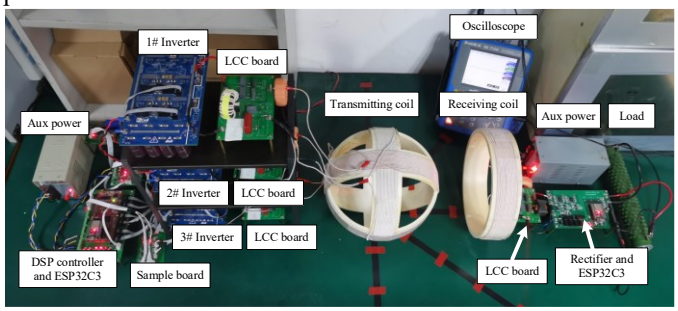

Fig. 10. DS-LCC OWPT experimental platform.

In order to verify the effectiveness of the proposed algorithm, the three receiving coil positions in Fig. 11 are compared, and the maximum transmission efficiency is

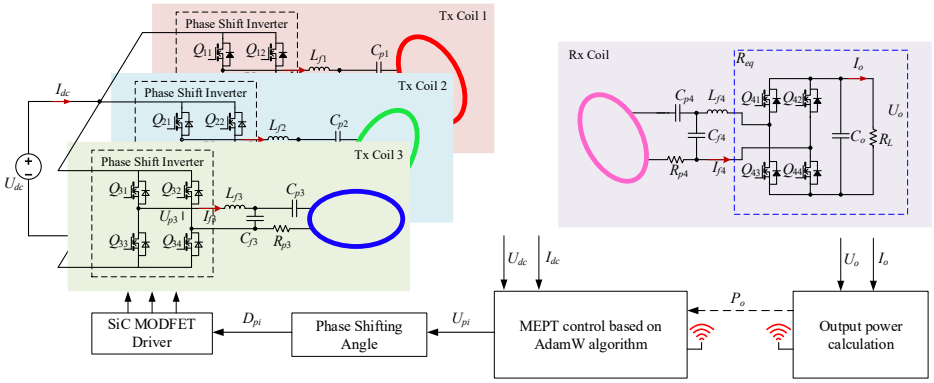

Fig. 9. The overall control block diagram of the system.

Authorized licensed use limited to: UNIVERSITY OF NOTTINGHAM. Downloaded on November 19,2024 at 15:19:26 UTC from IEEE Xplore. Restrictions apply.
© 2024 IEEE. Personal use is permitted, but republication/redistribution requires IEEE permission. See https://www.ieee.org/publications/rights/index.html for more information.

This article has been accepted for publication in IEEE Transactions on Power Electronics. This is the author's version which has not been fully edited and content may change prior to final publication. Citation information: DOI 10.1109/TPEL.2024.3486048

obtained when the receiving coil maintains a constant 20 W output power and achieves a constant power output.

TABLE II
EXPERIMENTAL PLATFORM PARAMETERS

Symbol	Quantity	Value
L_{p1}, L_{p2}, L_{p3}, L_{p4}	Transmitting and Receiving coils self-inductance	108.8 μH, 108 μH, 107 μH, 107.03 μH
L_{f1}, L_{f2}, L_{f3}, L_{f4}	Series compensation inductance	5 μH, 5.1 μH, 5 μH, 5 μH
C_{f1}, C_{f2}, C_{f3}, C_{f3}	Series compensation capacitance	125.2 nF, 126.6 nF, 125.2 nF, 126.3 nF
C_{p1}, C_{p2}, C_{p3}, C_{p4}	Transmitting and Receiving coils series compensation capacitance	5.49 nF, 6.02 nF, 6.20 nF, 6.1 nF
R_{p1}, R_{p2}, R_{p3}, R_{p4}	Coil internal resistance	0.15 Ω
C_o	Output capacitance	220 μF
R_L	Load resistance	5 Ω
U_{dc}	DC side input voltage	38 V
U_o	Load voltage	10 V
P_{load}	Output power	20 W
f_0	Switching frequency	200 kHz
r	Coil radius	12.5 cm
N	Number of coil turns	17

The position information of the receiving coil at position P(1) is $\varphi = 0°$, $\theta = 90°$, $d = 25$ cm, the information at position P(2) is $\varphi = 45°$, $\theta = 90°$, $d = 25$ cm, and the information at position P(3) is $\varphi = 45°$, $\theta = 90°$, $d = 28$ cm.

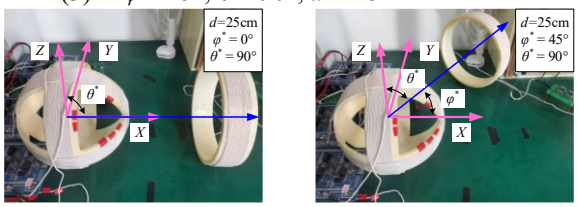

(a) (b)

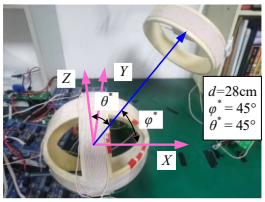

(c)

Fig. 11. Different receiving coil positions of OWPT system. (a, b, c) Receiving coil at position P(1), P(2) and P(3), respectively.

A. Steady-state characteristic

The experimental waveforms of the system at position P(1), P(2), and P(3) are shown in Fig. 12.

1. Position P(1) ($\varphi = 0°$, $\theta = 90°$, $d = 25$ cm)

When the receiving coil is at position P(1), after AdamW algorithm converges, the waveforms of the output voltages u_{pi}, the current i_{f1} of the inverter 1, the currents i_{pi} of transmitting and receiving coils, and the output voltage u_o of the load are shown in Fig. 12 (a).

At this time, the system is powered by the transmitting coil 1 for the load coil resistance. The RMS current values of the transmitting coil are $I_{p1} \approx 2.9$ A, $I_{p2} \approx 0.1$ A, $I_{p3} \approx 0.1$ A, and the receiving coil current $I_{p4} \approx 1.8$ A. The voltage on the load $u_o \approx 10.0$ V. The input power of the system is 27.4 W, the output power is 20.0 W, and the overall transmission efficiency of the system is 72.9 %.

2. Position P(2) ($\varphi = 45°$, $\theta = 90°$, $d = 25$ cm)

When the receiving coil is at position P(2), after AdamW algorithm converges, the waveforms of the output voltages u_{pi}, the current i_{f1} of the inverter 1, the currents i_{pi} of transmitting and receiving coils, and the output voltage u_o of the load are shown in Fig. 12 (b).

At this time, the coil is located between two transmitting coils, and the maximum transmission efficiency can be

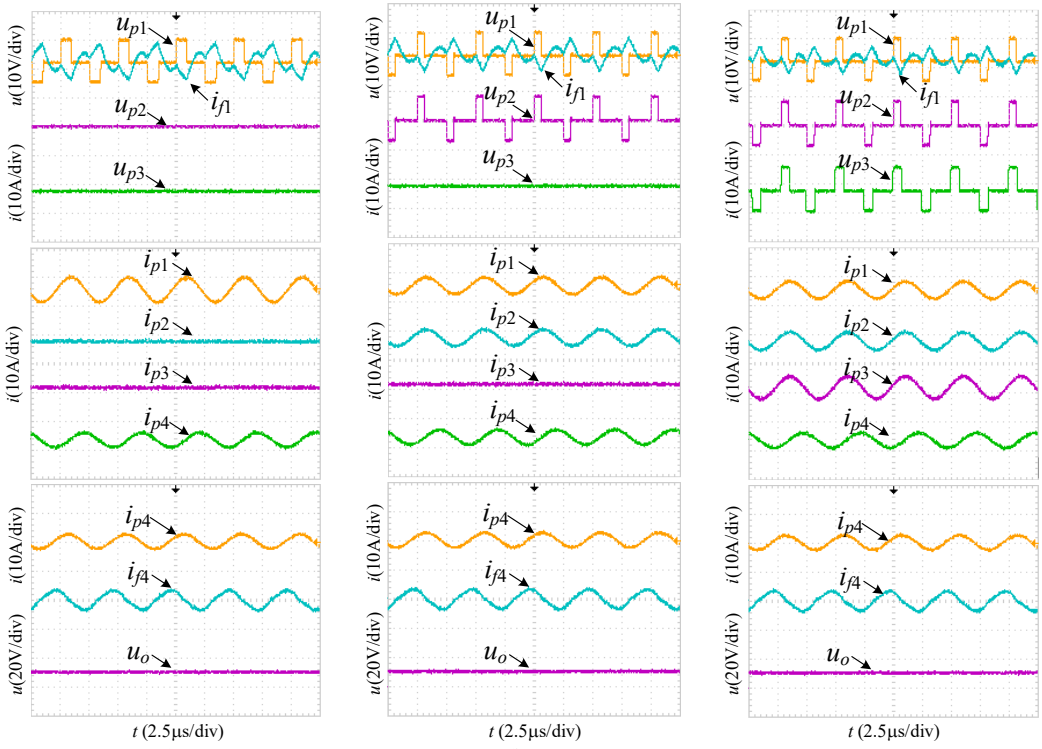

(a) (b) (c)

Fig. 12. The experimental waveforms of receiving coil at different positions. (a, b, c) Receiving coil at position P(1), P(2) and P(3), respectively.

Authorized licensed use limited to: UNIVERSITY OF NOTTINGHAM. Downloaded on November 19,2024 at 15:19:26 UTC from IEEE Xplore. Restrictions apply.
© 2024 IEEE. Personal use is permitted, but republication/redistribution requires IEEE permission. See https://www.ieee.org/publications/rights/index.html for more information.

This article has been accepted for publication in IEEE Transactions on Power Electronics. This is the author's version which has not been fully edited and content may change prior to final publication. Citation information: DOI 10.1109/TPEL.2024.3486048

achieved through the simultaneous power supply of the two transmitting coils. The RMS current values of the transmitting coil are $I_{p1} \approx 2.0$ A, $I_{p2} \approx 1.8$ A, $I_{p3} \approx 0.1$ A, and the receiving coil current $I_{p4} \approx 1.8$ A. The voltage on the load $u_o \approx 10.0$ V. The input power of the system is 26.9 W, the output power is 20.0 W, and the overall transmission efficiency of the system is 74.4 %.

3. Position P(3) ($\varphi = 45$ °, $\theta = 45$ °, $d = 28$ cm)

Also at position P(3), the current of coils are $I_{p1} \approx 2.0$ A, $I_{p2} \approx 2.1$ A, $I_{p3} \approx 2.4$ A, $I_{p4} \approx 1.8$ A, and the output voltage $u_o \approx 10.1$ V, as shown in Fig. 12 (c). The input power of the system is 30.4 W, the output power is 20.4 W, and the overall transmission efficiency of the system is 67.1 %.

At this time, power is supplied to the receiving coil through three transmitting coils, but the transmission efficiency of the system decreases due to the distance between the receiving coils.

B. Dynamic characteristic

In order to satisfy the different expected output power of the system and the constant power output under different loads, when the receiving coil at P(3), the dynamic characteristics of the system algorithm are verified by the sudden change of the expected power and the sudden change of the load.

1. Power sudden change characteristics.

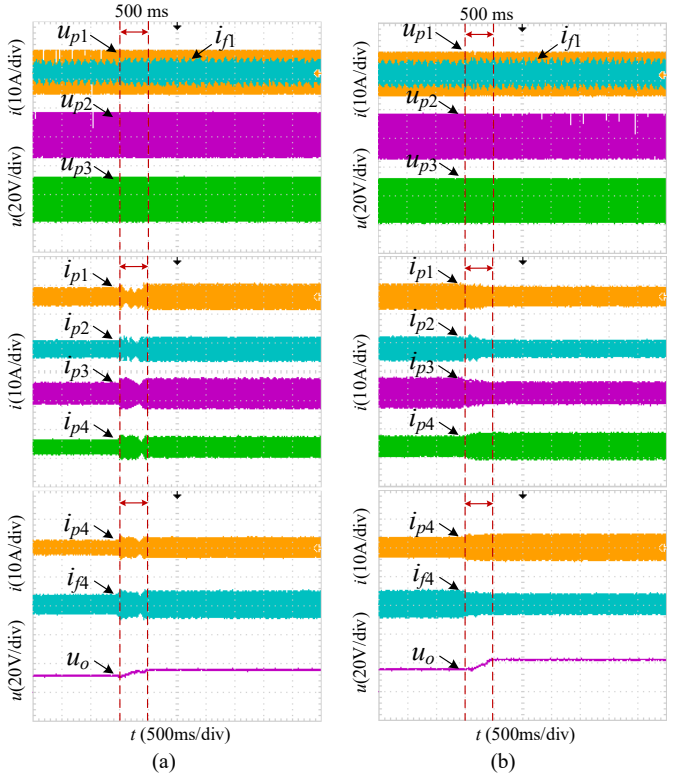

Fig. 13. System dynamic performance under AdamW algorithm. (a) Power sudden change waveforms. (b) Load sudden change waveforms.

Fig. 13 (a) shows the search process of output power sudden change from 20 W to 40 W while the load is 5 Ω. The RMS current values of the transmitting coil are $I_{p1} \approx 2.0$ A, $I_{p2} \approx 2.1$ A, $I_{p3} \approx 2.4$ A, and the receiving coil current $I_{p4} \approx 1.8$ A when the output power at 20 W. $I_{p1} \approx 2.9$ A, $I_{p2} \approx 2.9$ A, $I_{p3} \approx 3.4$ A and $I_{p4} \approx 2.3$ A when the output power at 40 W.

The convergence time of the system is about 500 ms, the stable output voltage u_o changes from 10.1 V to 14.2 V. The output power of the system changes from 20.4 W to 40.3 W, and the input power changes from 30.4W to 60.2 W. The efficiency of the system is 66.9 %.

2. Load sudden change characteristics.

Fig. 13 (b) shows the change process of system load from 5 Ω to 10 Ω when the constant power output is 40 W. The RMS current values of the transmitting coil are $I_{p1} \approx 2.9$ A, $I_{p2} \approx 2.8$ A, $I_{p3} \approx 3.4$ A, and the receiving coil current $I_{p4} \approx 2.3$ A when the load is 5 Ω. $I_{p1} \approx 2.2$ A, $I_{p2} \approx 2.1$ A, $I_{p3} \approx 2.5$ A and $I_{p4} \approx 3.1$ A when the load is 10 Ω.

The convergence time of the system is about 500 ms, and the stable output voltage u_o changes from 14.2 V to 20.3 V. The output power of the system is 40.3 W and becomes 41.2 W basically unchanged. The input power changes from 60.5 W to 54.1 W. The efficiency of the system is 76.2 %.

This is consistent with the analysis in part **III** section ***B. MEPT for load changes***. When two or more coils supply power to the receiving coil at the same time, the optimal transmission efficiency of the system can be achieved by combining the transmitting coil current sizes.

3. Dynamic characteristic with GD algorithm.

In order to compare the dynamic performance of different algorithms, experiments were also conducted to verify the power and load mutations of the GD algorithm. The experimental waveform is shown in Fig. 14. When the output power suddenly changes in Fig. 14 (a), the convergence time of the GD algorithm is about 1.5 s. When the load size suddenly changes in Fig. 14 (b), the convergence time of the GD algorithm is about 2 s. At the same initial step size, the convergence speed of GD algorithm is slower compared to AdamW algorithm, which is consistent with the simulation results. But both algorithms can achieve stable final output voltage.

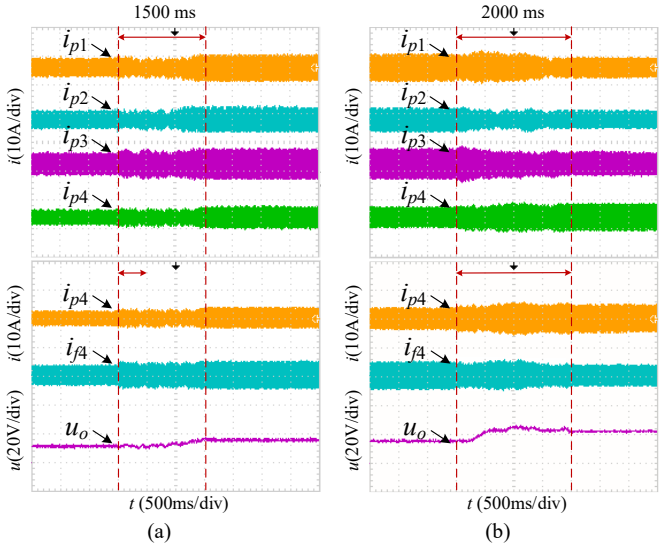

Fig. 14. System dynamic performance under GD algorithm. (a) Power sudden change waveforms. (b) Load sudden change waveforms.

C. Transmission characteristic

In order to verify the transmission characteristics of the

Authorized licensed use limited to: UNIVERSITY OF NOTTINGHAM. Downloaded on November 19,2024 at 15:19:26 UTC from IEEE Xplore. Restrictions apply.
© 2024 IEEE. Personal use is permitted, but republication/redistribution requires IEEE permission. See https://www.ieee.org/publications/rights/index.html for more information.

This article has been accepted for publication in IEEE Transactions on Power Electronics. This is the author's version which has not been fully edited and content may change prior to final publication. Citation information: DOI 10.1109/TPEL.2024.3486048

system, by stabilizing the output power to constant power 20 W output, select the receiving coil at different positions for measurement. In order to maximize the output power of the whole system, the input voltage of the transmitter coil is controlled by AdamW algorithm to adjust the current of the transmitter coil on the transmitting side, so as to achieve constant power control and maximum efficiency control of the load. The transmission efficiency curve of the system is shown in Fig. 15. When the receiving coil is in different positions, the output power of the system can achieve a constant output.

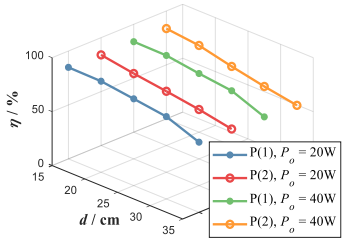

Fig. 15. Distance and transmission efficiency change curves at different output power, with the receiving coil in position 1 and 2 directions.

When the distance between the transmitting coil and the receiving coil is 15 cm, the maximum transmission efficiency of the system can reach 84.84%. As the distance between the coils increases, the maximum transmission efficiency of the coils decreases gradually. When the distance between the receiving coil and the transmitting coil is the same, the maximum transmission efficiency obtained is basically the same even if the receiving coil is at different positions (such as positions P(1) and P(2)).

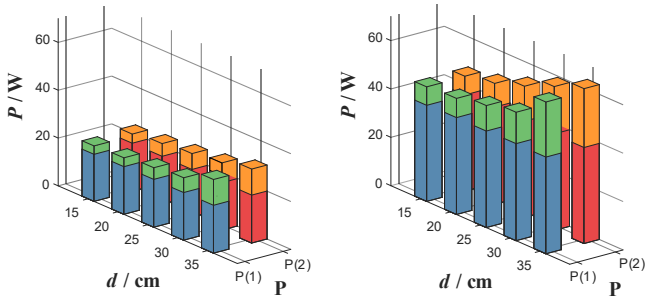

Fig. 16. Constant power output under the different distance of the output power, system loss and the input power. (a) P_o = 20W. (b) P_o = 40W.

Fig. 16 shows the system output power, system loss and input power at different distances in P(1) and P(2) directions. It can be seen that when the receiving coil distance gradually increases, the coupling coefficient of the system also decreases, and in order to make the load receive a constant output power, it is necessary to increase the input DC voltage to increase the current of transmitting coil. However, as the current increases, the transmitting coil's coil loss and the inverter's power increase, reducing overall transmission efficiency.

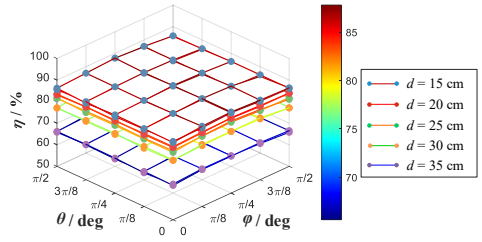

Fig. 17. Transmission efficiency curve of the system at different coil angles and transmission distances.

The efficiency tracking results of the receiving coil at different angles and transmission distances are plotted, as shown in Fig. 17. Due to the polar coordinate representation of the position of the receiving coil in space, where θ represents the angle with the Z-axis and φ represents the angle with the X-axis, as shown in Fig. 4. From Fig. 17, it can be seen that when the transmission distance of the receiving coil is constant, the transmission efficiency of the receiving coil varies slightly at different spatial angles, which is related to measurement errors and the direction of the synthesized magnetic vector of the coil. However, the transmission efficiency is basically the same at the same transmission distance. In addition, the transmission efficiency of the system mainly depends on the distance between the coils. As the transmission distance increases, the efficiency decreases.

Table III shows the comparison of transmission performance of some current omnidirectional wireless transmission systems. Compared with other power control methods, this paper has a better effect in tracking and controlling the maximum efficiency point under constant power output.

V. Conclusion

Based on the OWPT mathematical model, this paper analyzes the relationship between the input voltage, transmission power and transmission efficiency of the system. This work proposes a maximum efficiency point tracking control method based on AdamW algorithm. By detecting the output power of the system and adjusting the voltage on the input side, the maximum transmission efficiency and constant power of the system is obtained simultaneously. The experimental part verifies the static transmission characteristics and dynamic transmission characteristics of the system which can achieve maximum efficiency in any direction within 500 ms, proving the effectiveness of the

TABLE III
Performance Comparisons of OWPT System

Reference	Power	Efficiency	Type	Transmitter and receiver coil size	Distance
[22]	37.08 W	70.39 %	Cylindrical orthogonal transmitter	328, 150 mm	-
[23]	-	60 %	Cubic spiral transmitter	120, 20 mm	150 mm
[24]	20 W	85 %	Spherical orthogonal receiver	180, 180 mm	110 mm
[25]	36.9 W	30.6 %	Cylindrical orthogonal transmitter with multi receiver	328, 98 mm	210 mm
[26]	-	70 %	Spherical orthogonal transmitter with multi receiver	400, 100 mm	100 mm
This work	20 W	84.84 %	Spherical orthogonal transmitter	250, 250 mm	150 mm

Authorized licensed use limited to: UNIVERSITY OF NOTTINGHAM. Downloaded on November 19,2024 at 15:19:26 UTC from IEEE Xplore. Restrictions apply.
© 2024 IEEE. Personal use is permitted, but republication/redistribution requires IEEE permission. See https://www.ieee.org/publications/rights/index.html for more information.

This article has been accepted for publication in IEEE Transactions on Power Electronics. This is the author's version which has not been fully edited and content may change prior to final publication. Citation information: DOI 10.1109/TPEL.2024.3486048

maximum efficiency tracking method based on AdamW algorithm. Compared to traditional methods of adding DC/DC converters, the MEPT algorithm of OWPT system based on AdamW algorithm proposed in this paper can effectively improve the transmission efficiency of the system, and the highest efficiency can reach 84.84% at a transmission distance of 15 cm.

REFERENCES

[1] Chun T. Rim; Chris Mi, "Introduction to Wireless Power Transfer (WPT)," *Wireless Power Transfer for Electric Vehicles and Mobile Devices*, IEEE, 2017, pp.19-42.

[2] Z. Li, C. Zhu, J. Jiang, K. Song and G. Wei, "A 3-kW Wireless Power Transfer System for Sightseeing Car Supercapacitor Charge," *IEEE Transactions on Power Electronics*, vol. 32, no. 5, pp. 3301-3316, May. 2017.

[3] X. Ji, P. Zhao, H. Wang, H. Yang and M. Fu, "Multiple-Receiver Inductive Power Transfer System Based on Multiple-Coil Power Relay Module," *IEEE Transactions on Circuits and Systems I: Regular Papers*, vol. 70, no. 6, pp. 2625-2634, Jun. 2023.

[4] T. Feng, Y. Sun, Z. Zuo, Z. Wang and X. Dai, "Magnetic Field Analysis and Excitation Currents Optimization for an Omnidirectional WPT System Based on Three-Phase Tubular Coils," *IEEE Transactions on Industry Applications*, vol. 58, no. 1, pp. 1268-1278, Jan.-Feb. 2022.

[5] N. Ha-Van and C. Seo, "Analytical and Experimental Investigations of Omnidirectional Wireless Power Transfer Using a Cubic Transmitter," *IEEE Transactions on Industrial Electronics*, vol. 65, no. 2, pp. 1358-1366, Feb. 2018.

[6] C. Zhang, D. Lin and S. Y. Hui, "Basic Control Principles of Omnidirectional Wireless Power Transfer," *IEEE Transactions on Power Electronics*, vol. 31, no. 7, pp. 5215-5227, Jul. 2016.

[7] Z. Dai, J. Wang and C. Wang, "Output-Voltage Adaptive of Omnidirectional Wireless Power Transfer Based on Receivers With Digital Coils," *IEEE Journal of Emerging and Selected Topics in Power Electronics*, vol. 10, no. 4, pp. 4937-4945, Aug. 2022.

[8] H. Li, J. Li, K. Wang, W. Chen and X. Yang, "A Maximum Efficiency Point Tracking Control Scheme for Wireless Power Transfer Systems Using Magnetic Resonant Coupling," *IEEE Transactions on Power Electronics*, vol. 30, no. 7, pp. 3998-4008, Jul. 2015.

[9] X. Tang, J. Zeng, K. P. Pun, S. Mai, C. Zhang and Z. Wang, "Low-Cost Maximum Efficiency Tracking Method For Wireless Power Transfer Systems," in *IEEE Transactions on Power Electronics*, vol. 33, no. 6, pp. 5317-5329, Jun. 2018.

[10] H. Li, K. Wang, J. Fang and Y. Tang, "Pulse Density Modulated ZVS Full-Bridge Converters for Wireless Power Transfer Systems," *IEEE Transactions on Power Electronics*, vol. 34, no. 1, pp. 369-377, Jan. 2019.

[11] M. Fu, H. Yin, M. Liu and C. Ma, "Loading and Power Control for a High-Efficiency Class E PA-Driven Megahertz WPT System," *IEEE Transactions on Industrial Electronics*, vol. 63, no. 11, pp. 6867-6876, Nov. 2016.

[12] W. X. Zhong and S. Y. R. Hui, "Maximum Energy Efficiency Tracking for Wireless Power Transfer Systems," *IEEE Transactions on Power Electronics*, vol. 30, no. 7, pp. 4025-4034, Jul. 2015.

[13] L. Zhou *et al*., "Efficiency Optimization of LCC-S Compensated Multiple-Receiver Bidirectional WPT System for Stackers in Automated Storage and Retrieval Systems," *IEEE Transactions on Power Electronics*, vol. 37, no. 12, pp. 15693-15705, Dec. 2022.

[14] Kingma, D., and Ba, J., "Adam: A Method for Stochastic Optimization," *arXiv preprint arXiv:*1412.6980 (2014).

[15] Ilya. L, and Frank. H, "Decoupled Weight Decay Regularization," *arXiv preprint arXiv:* 1711.05101 (2019).

[16] H. Wu, J. Zhao, F. Wang, L. Bai, B. Luo and J. You, "Parameter Identification of Underwater Wireless Power Transfer System Based on Adam Optimization Algorithm," 2024 *IEEE 10th International Power Electronics and Motion Control Conference* (*IPEMC2024-ECCE Asia*), Chengdu, China, 2024, pp. 4626-4630.

[17] K. Ding, N. Xiao, K. Toh, "Adam-family Methods with Decoupled Weight Decay in Deep Learning," *arXiv preprint arXiv:* 2310.08858 (2023).

[18] H. T. Nguyen *et al*., "Review Map of Comparative Designs for Wireless High-Power Transfer Systems in EV Applications: Maximum Efficiency, ZPA, and CC/CV Modes at Fixed Resonance Frequency Independent From Coupling Coefficient," *IEEE Transactions on Power Electronics*, vol. 37, no. 4, pp. 4857-4876, Apr. 2022.

[19] H. Dan *et al*., "An Extremum Seeking Algorithm Based on Square Wave for Three-Dimensional Wireless Power Transfer System to Achieve Maximum Power Transmission," *IEEE Transactions on Industry Applications*, vol. 58, no. 1, pp. 1279-1288, Jan.-Feb. 2022.

[20] Z. Liu, M. Su, Q. Zhu, Y. Chao, S. Zang and A. P. Hu, "A Dual-Frequency 3-D WPT System With Directional Power Transfer Capability at Two Separately Regulated Outputs," *IEEE Journal of Emerging and Selected Topics in Power Electronics*, vol. 11, no. 3, pp. 2514-2524, Jun. 2023.

[21] T. Kan, T. -D. Nguyen, J. C. White, R. K. Malhan and C. C. Mi, "A New Integration Method for an Electric Vehicle Wireless Charging System Using LCC Compensation Topology: Analysis and Design," *IEEE Transactions on Power Electronics*, vol. 32, no. 2, pp. 1638-1650, Feb. 2017.

[22] M. Su, Z. Liu, Q. Zhu and A. P. Hu, "Study of Maximum Power Delivery to Movable Device in Omnidirectional Wireless Power Transfer System," *IEEE Access*, vol. 6, pp. 76153-76164, 2018.

[23] H. Wang *et al.*, "Omnidirectional magnetic resonant coupling wireless power transfer system with a cubic spiral transmitter," *AIP Advances*. 9. 06521, 2019.

[24] X. Tian, K. T. Chau, W. Liu and C. H. T. Lee, "Analysis of Multi-Coil Omnidirectional Energy Harvester," *IEEE Transactions on Magnetics*, vol. 57, no. 2, pp. 1-6, Feb. 2021.

[25] H. Han, Z. Mao, Q. Zhu, M. Su and A. P. Hu, "A 3D Wireless Charging Cylinder With Stable Rotating Magnetic Field for Multi-Load Application," *IEEE Access*, vol. 7, pp. 35981-35997, 2019.

[26] Z. Zhu et al., "Efficiency Optimization and Power Allocation of Omnidirectional Wireless Power Transfer for Multiple Receivers," *IEEE Transactions on Industrial Electronics*, vol. 70, no. 10, pp. 9689-9699, Oct. 2023.

Authorized licensed use limited to: UNIVERSITY OF NOTTINGHAM. Downloaded on November 19,2024 at 15:19:26 UTC from IEEE Xplore. Restrictions apply.
© 2024 IEEE. Personal use is permitted, but republication/redistribution requires IEEE permission. See https://www.ieee.org/publications/rights/index.html for more information.